© 2018. Published by The Company of Biologists Ltd | Journal of Experimental Biology (2018) 221, jeb190892. doi:10.1242/jeb.190892

RESEARCH ARTICLE

Hydrodynamics of linear acceleration in bluegill sunfish, *Lepomis macrochirus*

Tyler N. Wise, Margot A. B. Schwalbe* and Eric D. Tytell‡

ABSTRACT

In their natural habitat, fish rarely swim steadily. Instead they frequently accelerate and decelerate. Relatively little is known about how fish produce extra force for acceleration in routine swimming behavior. In this study, we examined the flow around bluegill sunfish *Lepomis macrochirus* during steady swimming and during forward acceleration, starting at a range of initial swimming speeds. We found that bluegill produce vortices with higher circulation during acceleration, indicating a higher force per tail beat, but they do not substantially redirect the force. We quantified the flow patterns using high speed video and particle image velocimetry and measured acceleration with small inertial measurement units attached to each fish. Even in steady tail beats, the fish accelerates slightly during each tail beat, and the magnitude of the acceleration varies. In steady tail beats, however, a high acceleration is followed by a lower acceleration or a deceleration, so that the swimming speed is maintained; in unsteady tail beats, the fish maintains the acceleration over several tail beats, so that the swimming speed increases. We can thus compare the wake and kinematics during single steady and unsteady tail beats that have the same peak acceleration. During unsteady tail beats when the fish accelerates forward for several tail beats, the wake vortex forces are much higher than those at the same acceleration during single tail beats in steady swimming. The fish also undulates its body at higher amplitude and frequency during unsteady tail beats. These kinematic changes likely increase the fluid dynamic added mass of the body, increasing the forces required to sustain acceleration over several tail beats. The high amplitude and high frequency movements are also likely required to generate the higher forces needed for acceleration. Thus, it appears that bluegill sunfish face a trade-off during acceleration: the body movements required for acceleration also make it harder to accelerate.

KEY WORDS: Locomotion, Unsteady swimming, Particle image velocimetry, Wake structure

INTRODUCTION

Many previous studies of the mechanics of fish swimming have focused on steady locomotion. But in nature, fish do not usually swim steadily. Instead, they rely on unsteady swimming maneuvers and changes in direction (Webb, 1991). Previous studies have examined some unsteady maneuvers such as C- and S-starts (Domenici and Blake, 1997), but relatively few have looked at the hydrodynamics of linear accelerations. To better understand natural motion of fish, it is necessary to understand how fish accelerate. Similarly, in order to accurately replicate natural swimming motions in man-made robotic systems, it is necessary to look at the forces during these natural behaviors.

The kinematics and hydrodynamics of acceleration in a variety of fish species were recently surveyed (Akanyeti et al., 2017). Across 51 species, they reported a consistent, large increase in tail beat amplitude and frequency. They also studied the wake of rainbow trout in detail, and showed that the kinematic changes lead to an increase in the impulse in vortex rings in the wake and a reorientation of the rings, indicating that the force is reoriented to be more axially directed, rather than laterally. They found that the rings become more circular, which would result in a more hydrodynamically efficient transfer of force into the wake (Akanyeti et al., 2017). Trout swim in a subcarangiform mode, meaning that they undulate primarily their tail and have a relatively long body wavelength (Lauder and Tytell, 2005). During each tail beat, they shed two single vortices in a pattern called a 2S wake (Koochesfahani, 1989). The hydrodynamics of acceleration has also been studied in American eels (Tytell, 2004a), a fish that swims differently to trout, in an anguilliform mode, which means that they undulate most of their bodies during steady swimming and have a relatively short undulatory wavelength (Lauder and Tytell, 2005), producing two pairs of vortices each tail beat in a pattern called a 2P wake (Koochesfahani, 1989). The vortex pairs each produce a jet that is directed laterally. During acceleration, the eels reoriented the vortex pairs so that the jets pointed away from the fish, more in the axial direction (Tytell, 2004a).

In this study, we examined the kinematics and hydrodynamics of acceleration in the bluegill sunfish, a carangiform swimmer that produces a similar 2S wake to the trout, but a different one to the eel. Carangiform swimmers have longer body wavelengths than anguilliform swimmers and tend to have lower amplitude oscillations in the anterior body. During steady swimming, bluegill, like trout, produce a 2S wake, with a single pair of vortices per tail beat cycle (Drucker and Lauder, 2000; Lauder and Tytell, 2005; Tytell, 2007). In this type of wake, the jets between the vortex pairs point away from the fish even during steady swimming (Fig. 1A).

The steady wake structures of the bluegill and the eel suggest that they produce locomotor force in somewhat different ways. When a fish is swimming steadily, and acceleration is zero, the net force on the body should average out to zero over a tail beat cycle and over the entire body. This is equivalent to saying that the thrust force has to equal the drag force, on average. If the net force is zero, then there should not be any axial momentum in the fish's wake. Using the wake to estimate the forces on a body in a fluid is a standard fluid dynamic technique, called a control volume analysis (Smits, 2000). For a steadily swimming eel, there is no net axial momentum in its wake, as would be expected by a control volume analysis

Department of Biology, Tufts University, 200 Boston Ave, Suite 4700, Medford, MA 02155, USA.
*Present address: Department of Biology, Lake Forest College, 555 North Sheridan Road, Lake Forest, IL 60045, USA.

‡Author for correspondence (eric.tytell@tufts.edu)

T.N.W., 0000-0002-7956-1809; M.A.B.S., 0000-0003-1652-0775; E.D.T., 0000-0002-6603-9448

Received 17 August 2018; Accepted 28 September 2018

Journal of Experimental Biology (2018) 221, jeb190892. doi:10.1242/jeb.190892

List of symbols and abbreviations

$\mathbf{a}_{dyn}$	dynamic acceleration vector of the fish's center of mass (m s^{-2})
a_{peak}	peak dynamic acceleration in the axial direction for each half tail beat (BL s^{-1})
$\mathbf{a}_{total}$	total acceleration vector, the sum of gravitational and dynamic acceleration (m s^{-2})
BL	body length (cm)
C_A	added mass coefficient
C_D	drag coefficient
d	vortex ring diameter in the horizontal plane (cm)
D	vortex ring diameter in the vertical plane (cm)
$\mathbf{F}_{accel}$	force required for acceleration (N)
$\mathbf{F}_{axial}$	wake force in the axial (swimming) direction (N)
$\mathbf{F}_{drag}$	force to overcome drag (N)
$\mathbf{F}_{total}$	total wake force magnitude (N)
$\boldsymbol{g}$	gravitational acceleration vector (m s^{-2})
m	mass of the fish (g)
S	surface area of the fish (cm^2)
T	tail beat period (s)
T_i	time of peak lateral excursion for tail beat i (s)
U	swimming speed (BL)
$\mathbf{u}$	flow speed vector (cm s^{-1})
Γ	circulation of vortices in the wake (cm^2 s^{-1})
θ	angle of vortex rings in the wake (deg)
ρ	density of water (kg m^{-3})

(Tytell, 2007). In contrast, when a bluegill is swimming steadily, its wake contains a strong axial jet (Lauder and Tytell, 2005; Lauder et al., 2003; Tytell, 2007) (Fig. 1A). This might make it appear that thrust is not equal to drag during steady locomotion. This apparent discrepancy can be explained in several ways, as discussed in detail by Tytell (2007). First of all, a carangiform swimmer produces primarily thrust with its tail and primarily drag with its anterior body (Bale et al., 2014a; Borazjani and Sotiropoulos, 2008; DuBois, 1978; DuBois et al., 1974). This spatial segregation of forces is similar to a boat with a propeller. An average over a full control volume would show a net zero axial momentum, but flow behind the hull will show net drag and flow behind the propeller would show net thrust. Similarly, for the bluegill, the wake close to the tail may mostly represent thrust from the tail (Tytell, 2007). Since eels do not segregate force production as much, their wake, even close to the tail, represents more of an overall average, and shows no net axial flow. Second, steady swimming is not actually steady; each tail beat during steady locomotion is really a small acceleration and deceleration (Borazjani and Sotiropoulos, 2008; Tytell, 2007; Xiong and Lauder, 2014), and bluegill accelerate and decelerate more during steady swimming motions than eels (Tytell, 2007). The axial jets in their steady wake structure may represent the force needed for each small acceleration.

To accelerate, the fish must increase the axial force (Fig. 1). Based on the wake structure during steady locomotion, there are two primary ways to increase the axial force generated. The axial force is:

$$\mathbf{F}_{axial} = \mathbf{F}_{total} \sin\theta. \quad (1)$$

The fish could reorient the total force, increasing θ, so that it points more in the axial direction (Fig. 1B), or it could increase the total force $\mathbf{F}_{total}$, which would be reflected by an increase in the vortex circulation Γ (Fig. 1C), or both. These two effects would cause characteristic changes in the wake. If the fish reorients the force, it will also reorient the vortex pairs in its wake, increasing the angle θ between the vortex pairs and the swimming direction, so that more of the resulting force is in the axial direction (Fig. 1B). For a bluegill, this angle is largely determined by the tail beat frequency, tail beat amplitude and swimming speed. For example, if swimming speed and tail beat amplitude stay the same but tail beat frequency increases, then the vortices will be closer together, which would lead to an increase in the angle θ. If the fish increases the total force, it will produce vortices with higher circulation Γ. In this case, the force vector might point in the same direction as it does during steady locomotion, but the total force would be greater, meaning that the axial component of the total force is also larger (Fig. 1C). Akanyeti et al. (2017) found that rainbow trout use both mechanisms; they produce more force and they reorient it more in the axial direction.

The increase in axial force must not only be large enough to accelerate the fish's own mass, but it must also push the fluid around it out of the way. This effect is called 'added mass' (Faber, 1995); it is as if the fish had a larger mass than only its body. For a carangiform fish like the bluegill, the tail must also produce enough force to overcome the drag on the body (Tytell, 2007). The axial force that the tail produces during acceleration is thus composed of two parts: the force to accelerate the mass of the body and the fluid around it, and the force to overcome the drag on the body.

$$\mathbf{F}_{axial} = \mathbf{F}_{accel} + \mathbf{F}_{drag}, \quad (2)$$

$$\mathbf{F}_{accel} = C_A m a_{dyn}, \quad (3)$$

$$\mathbf{F}_{drag} = \frac{1}{2} C_D \rho S U^2, \quad (4)$$

where C_A is the dimensionless added mass coefficient, m is the mass of the body, a_{dyn} is the dynamic acceleration, C_D is a dimensionless drag coefficient, ρ is the density of water, S is an area (commonly the surface area of the body) and U is the swimming speed. The added mass coefficient C_A is usually 1.0 or less for streamlined bodies (Daniel, 1984), and both it and the drag coefficient C_D may be different at different swimming speeds due to changes in tail beat frequency and amplitude or which fins the fish uses at different speeds.

Because bluegill are stiffer than eels or trout (Aleyev, 1977), we hypothesize that they may be less able than these fishes to achieve sufficiently high tail amplitudes to reorient vortices in the wake.

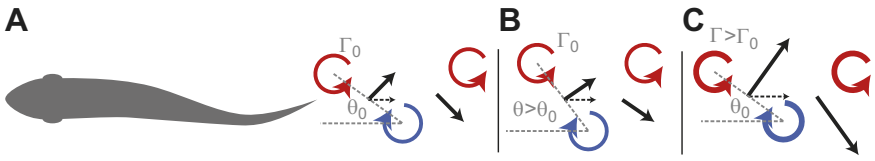

Fig. 1. Schematic showing how bluegill sunfish might produce more thrust during acceleration. Based on the steady swimming wake for a carangiform swimmer (A), the fish might produce more thrust by reorienting the tail force vector, which would be seen by an increase in θ for the vortex pairs in its wake (B), or by producing a larger force, which would be indicated by vortices with higher circulation Γ (C), or both. Red and blue arrows indicate vortices, where θ is the angle of a vortex pair to the swimming direction and Γ is the vortex circulation. The thick black arrows and dashed arrows indicate total force and thrust force, respectively.

Journal of Experimental Biology (2018) 221, jeb190892. doi:10.1242/jeb.190892

Additionally, because bluegill have relatively long body wavelengths compared with these fishes (Lauder and Tytell, 2005), greater tail amplitudes may not lead to larger spacing between vortices in the wake, but may simply cause the head to swing from side to side more, an effect called recoil (Lighthill, 1970). Together, these two features of bluegill swimming suggest that they may accelerate differently than eels or trout, increasing the force from each tail beat (Fig. 1C) rather than reorienting it.

In this study, we examined how bluegill sunfish produce forces during steady swimming and linear forward acceleration, which we term unsteady swimming. We quantified kinematics with high speed video, examined the wake using particle image velocimetry, and measured acceleration using an inertial measurement unit (IMU). For both steady and unsteady swimming, each tail beat contains forward acceleration (Tytell, 2007; Xiong and Lauder, 2014), which may be smaller or larger depending on the swimming mode and speed of the overall acceleration. This pattern allowed us to compare the forces and kinematics required for the same magnitude acceleration in isolated tail beats during steady swimming and sustained over several tail beats during unsteady swimming.

MATERIALS AND METHODS

Animals

Four bluegill (*Lepomis macrochirus* Rafinesque 1810) were captured by beach seine in White Pond, Concord, MA, USA. All animals were housed individually in 38 l aquaria with a 12 h:12 h light:dark cycle and were fed live worms or flake food (earthworm flake, Pentair, Apopka, FL, USA) daily. Water temperature (20±2°C) and pH (7.4) were kept constant and were equal to that used during experiments. Fish total length ranged from 148 to 163 mm (mean±s.d.=155±7 mm) and mass ranged from 54 to 78 g (70±11 g). Animal care and all experimental procedures followed a protocol approved by Tufts University (M2012-145 and M2015-149).

Particle image velocimetry

Flows generated by the swimming fish were quantified using particle image velocimetry (PIV) (Tytell, 2011). Neutrally buoyant glass particles (50 µm diameter, TSI, Ypsilanti, MI, USA) were placed in a 293 l flow tank (Loligo Systems, Viborg, Denmark) and were illuminated with two 5W 532 nm continuous lasers (Opus 532, Laser Quantum, Santa Clara, CA, USA). One laser was aimed directly at the viewing area in the flow tank (25×26 cm). The second laser projected a horizontal light sheet at a 45 deg mirror to increase the light intensity in viewing area (Fig. 2). The two light sheets were 6 cm from the bottom of the tank and the water depth was 30 cm. Video was recorded from below the flow tank with a high-speed camera (Phantom Miro M120, Vision Research, Wayne, NJ, USA) at 500 frames per second (Fig. 2).

Inertial measurement unit construction and attachment

An inertial measurement unit (IMU; MPU-9250, InvenSense Inc., San Jose, CA, USA) was attached to the fish's body to measure body orientation and dynamic acceleration. Fine, coated copper wires (80 µm diameter, Omega Engineering, Stamford, CT, USA) were soldered to individual pads on the IMU following the company's instruction for the serial peripheral interface (SPI). The IMU and copper wire connections were waterproofed by encasing them in epoxy (CircuitWorks Epoxy, Chemtronics, Kennesaw, GA, USA). Data were collected from the IMU by connecting it to a USB SPI interface (USB-8451, National Instruments, Austin, TX, USA) and viewed in a custom LabVIEW program (v. 2014, National Instruments). Before surgery, in order to account for drift of the IMU data, the IMU was suspended in water with no flow for 10 min. This was used to calibrate the drift during the trials.

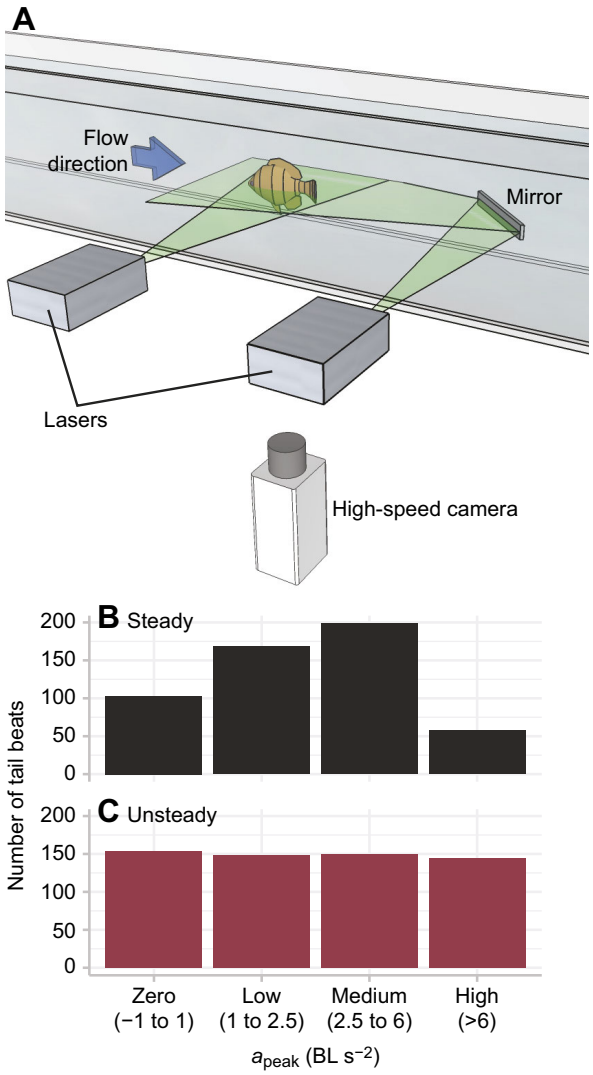

Fig. 2. Experimental setup and number of tail beats in each category. (A) A bluegill swims against the flow (blue arrow) in a flow tank. The fluid is illuminated by two lasers, one of which bounces off a mirror in the flow to illuminate the back side of the fish. A high-speed camera below the tank records motion of particles in the flow. (B,C) Steady (B) and unsteady (C) tail beats in four different acceleration categories.

An IMU was attached to each bluegill immediately before swimming experiments. Each fish was anesthetized with a buffered 0.02% solution of tricaine methane sulfonate (MS222, Sigma-Aldrich, St Louis, MO, USA). During surgery (~20 min), anesthesia was maintained by pumping buffered 0.01% MS222 over the fish's gills. The IMU was sutured just below and anterior to the dorsal fin, which is near the fish's center of mass, and a local anesthetic (bupivacaine USP, 1 mg kg^{-1}; Sigma-Aldrich) was injected in the suturing area.

Before the fish completely recovered from anesthesia, we calibrated the orientation of the IMU on the fish's body. The fish was placed in three known orientations (left side down in a horizontal orientation, dorsal side up in a normal swimming orientation, and nose down in a vertical orientation) to identify the three axes in the coordinate system.

Fish recovered from the surgery in a separate tank before being placed in the flow tank (~10 min). Fish acclimated to the flow tank for 1 h before experiments began. Upon completion of the experiments, fish were briefly anesthetized (0.01% buffered MS222) so that the IMU and sutures could be removed.

Swimming trials

Before each experiment, fish were acclimated to the flow tank and the laser sheets. Fish typically avoid the bright laser sheets and thus needed conditioning to acclimate to them. Fish were transported between their home tank and the flow tank to habituate to the experimental setup. Once in the flow tank, fish swam into the flow and were gently prodded into the laser sheets by placing dowels in front and behind the fish. This procedure was repeated several times over 4 days until each fish would swim steadily within the light sheets for extended periods of time.

During experimental trials, each fish swam at flow speeds between 1.0 and 2.5 body lengths per second (BL s^{-1}) in 0.5 BL s^{-1} intervals. Fish were confined to a 90-cm-long section of the 25×26×150 cm (height×width×length) working section of the flow tank. For each bluegill, at least three acceleration trials and three steady locomotion sequences were recorded at each flow speed. Each trial had at least five tail beats, and the fish did not turn more than 30 deg from its original position. During acceleration trials, we also recorded at least five tail beats, and all were analyzed.

We classified individual tail beats as 'steady' or 'unsteady' by measuring the motion of the fish in the laboratory frame of reference. When a fish is steadily matching the oncoming flow in the flow tank, its position is steady relative to the camera. A tail beat was classified as steady when a fish moved less than 2% of its body length over the course of the tail beat. Unsteady tail beats were those when it moved forward more than 2%, and we did not analyze tail beats in which the fish moved backward more than 2% of its body length.

Accelerations were induced in multiple ways. Fish were first positioned in the viewing area using a pair of dowels. Accelerations were initiated by either removing the dowel in front of the fish or dropping a heavy object (e.g. a D-cell battery) behind the fish. Care was taken to avoid any hydrodynamic interference with either acceleration inducing method and the dowels. Fish occasionally responded with a C-start to the dropping of the heavy object, and these were not included in the analysis. During all experiments, fish were maintained in the center of the viewing area of the flow tank since swimming near the walls can increase thrust, based on measurements of flapping foils (Fernández-Prats et al., 2015).

Data analysis

All custom code used for analysis and data processing is available online (http://dx.doi.org/10.6070/H4KS6Q5V).

Videos were processed with Insight 4G (TSI) to quantify fluid vorticity and velocity. The flow fields were processed using a custom MATLAB (R2014b, MathWorks) program. The center and diameter of vortices were manually identified and the circulation was calculated as:

$$\Gamma = \oint \mathbf{u} \cdot \mathrm{d}\mathbf{t}, \tag{5}$$

where $\mathbf{u}$ is the velocity vector and $\mathbf{t}$ is the unit vector tangent to the outline (Faber, 1995). The position data were used to calculate the orientation and distance in between each vortex pair. The mean total force, $\mathbf{F}_{\mathrm{total}}$, required to produce the vortex pair can be expressed by:

$$\mathbf{F}_{\mathrm{total}} = \frac{\pi\rho\ \Gamma D d}{4T}, \tag{6}$$

where ρ is the density of water, Γ is the average circulation of the two vortices, D is the distance between the two vortices in the horizontal plane, d is the height of the caudal fin and T is the tail beat period (Tytell, 2011). The tail beat period for each individual tail beat was found using custom MATLAB program to track the head and tail position of the fish over time.

The IMU measures angular velocities in three axes, and total acceleration $\mathbf{a}_{\mathrm{total}}$ along three axes. Total acceleration is the vector sum of dynamic acceleration vector $\mathbf{a}_{\mathrm{dyn}}$ due to the fish's movement and the gravitational acceleration vector $\boldsymbol{g}$:

$$\mathbf{a}_{\mathrm{total}} = \boldsymbol{g} + \mathbf{a}_{\mathrm{dyn}}. \tag{7}$$

To estimate just the dynamic acceleration, we use the algorithm developed by Madgwick et al. (2011) to estimate $\boldsymbol{g}$, which is the 3D orientation of the fish. Once the orientation is known, then the gravitational vector can be subtracted from the total acceleration to estimate dynamic acceleration. Briefly, the algorithm takes advantage of the fact that the IMU gives us two independent estimates of orientation. First, we can estimate orientation by integrating the angular velocities. This value tends to drift if angular velocities are low. But when angular velocities are low, dynamic accelerations also tend to be low, so that the total acceleration is close to the gravitational acceleration, which gives another estimate of orientation. By merging these two estimates in an optimal fashion, we can accurately estimate orientation (Madgwick et al., 2011) and from that estimate dynamic acceleration. The algorithm was implemented in a custom MATLAB script.

A custom MATLAB program allowed manual identification of the location of the tail tip and the tip of the snout. Based on these identified positions, the peak lateral excursion of the tail was identified, following procedures used previously (Tytell, 2004b). The tail beat amplitude is the distance from the midpoint to the peak excursion on either side. If t_i is the time of peak lateral excursion and t_{i-1} is the time of the previous peak, then the tail beat frequency at time i is $\frac{1}{2}(t_i - t_{i-1})$. Head amplitudes were identified in the same way. Peak accelerations a_{peak} in the forward direction were extracted from the dynamic acceleration from the IMU, which determined the peak acceleration for each half tail beat, the time interval between peak lateral tail excursion on one side to peak excursion on the other (from t_{i-1} to t_i).

Statistics

Our statistical models were based on the physical model in Eqns 2 and 3. We used a mixed model regression to compare how the total wake force depends on the swimming speed and acceleration. Although Eqn 2 represents a continuous relationship, neither total force nor acceleration were normally distributed, which would tend to result in biased or inaccurate regression coefficients. The distribution of total force was always positive, but had a long tail, making it appropriate for a log transformation. We then binned the peak acceleration a_{peak} in each half tail beat into four categories: zero ($-1 \leq a_{\mathrm{peak}} < 1$ BL s^{-2}), low ($1 \leq a_{\mathrm{peak}} < 2.5$ BL s^{-2}), medium ($2.5 \leq a_{\mathrm{peak}} < 6$ BL s^{-2}) and high ($a_{\mathrm{peak}} \geq 6$ BL s^{-2}). The boundaries between bins were chosen so that we had approximately the same number of unsteady acceleration tail beats in each bin. This procedure is similar to the ranking procedures that are the basis of most nonparametric statistics (Kloke and McKean, 2015). We also

Journal of Experimental Biology (2018) 221, jeb190892. doi:10.1242/jeb.190892

included the tail beat type s (steady versus unsteady) and the flow speed U in the model, along with the two-way interactions. Thus, the model for total force was:

$$\log F = \beta_0 + \beta_a(a_{bin}) + \beta_{vel}(U) + \beta_{steady}(s) + \beta_{a\times s}(a_{bin}, s) + \beta_{a\times U}(a_{bin}, U) + \beta_{U\times s}(U, s) + \gamma_k, \quad (8)$$

where β_0 is the intercept, $\beta_a(a_{bin})$ is related to the added mass coefficient for each acceleration bin, $\beta_{steady}(s)$ defines how unsteady tail beats are different from steady tail beats and $\beta_{vel}(U)$ indicates the effect of flow speed on total force. The interaction terms describe how total force may depend on the combinations of acceleration, tail beat type and swimming speed. We included a random effect γ_k, due to differences in individual fish.

We use the same model structure for vortex ring angle, diameter, tail beat frequency, and the head and tail amplitude. Tail beat frequency was also log transformed.

Regressions were performed in R (version 3.4.4) using the nlme package (version 3.1-131.1). Marginal means were estimated using the emmeans package (version 1.2.1). Figures were created using ggplot2 (version 2.2.1) and beeswarm plots with ggbeeswarm (version 0.6.0).

To test for robustness, we performed the same regressions with different numbers of acceleration bins, and with different ways of choosing the bin edges. The overall statistical patterns are the same, regardless of the bins.

Most figures use standard statistical box plots to show the distribution of the data, where the boxes span the 25th to the 75th percentile, with a line at the median, and whiskers represent 1.5 times the interquartile range.

RESULTS

We tested the hypothesis that bluegill sunfish produce axial force by increasing the total amount of force produced, as opposed to reorienting the forces in its wake. Data were recorded from four individuals at 1.0, 1.5 and 2.0 BL s^{-1}, and three individuals at 2.5 BL s^{-1}. One individual would not swim steadily at 2.5 BL s^{-1}. A total of 1122 vortex pairs and the accompanying kinematics were analyzed.

Because we measured acceleration directly, we quantified acceleration in both steady tail beats in which the fish matched speed against the flow and did not move more than 2% of its body length within the flow tank, and in unsteady tail beats in which the fish moved forward in the flow tank. Even in nominally steady tail beats, each tail beat includes an acceleration and deceleration, but in unsteady sequences, the fish maintains the acceleration over several tail beats, causing it to move forward in the tank. Fig. 2 shows the number of tail beats in each acceleration category for steady and unsteady sequences.

Fig. 3 shows examples of the flow patterns in the wake during steady swimming with a_{peak}=0.59 BL s^{-2} (Fig. 3A), and during two unsteady sequences, one with a medium acceleration with a_{peak}=4.75 BL s^{-2} (Fig. 3B), and the other with a high acceleration with a_{peak}=67.7 BL s^{-2} (Fig. 3C). The corresponding video sequences are available in Movies 1–3. The wake consists of vortices that alternate in rotational direction, represented by red and blue colors on the figure. This created backward jets of fluid

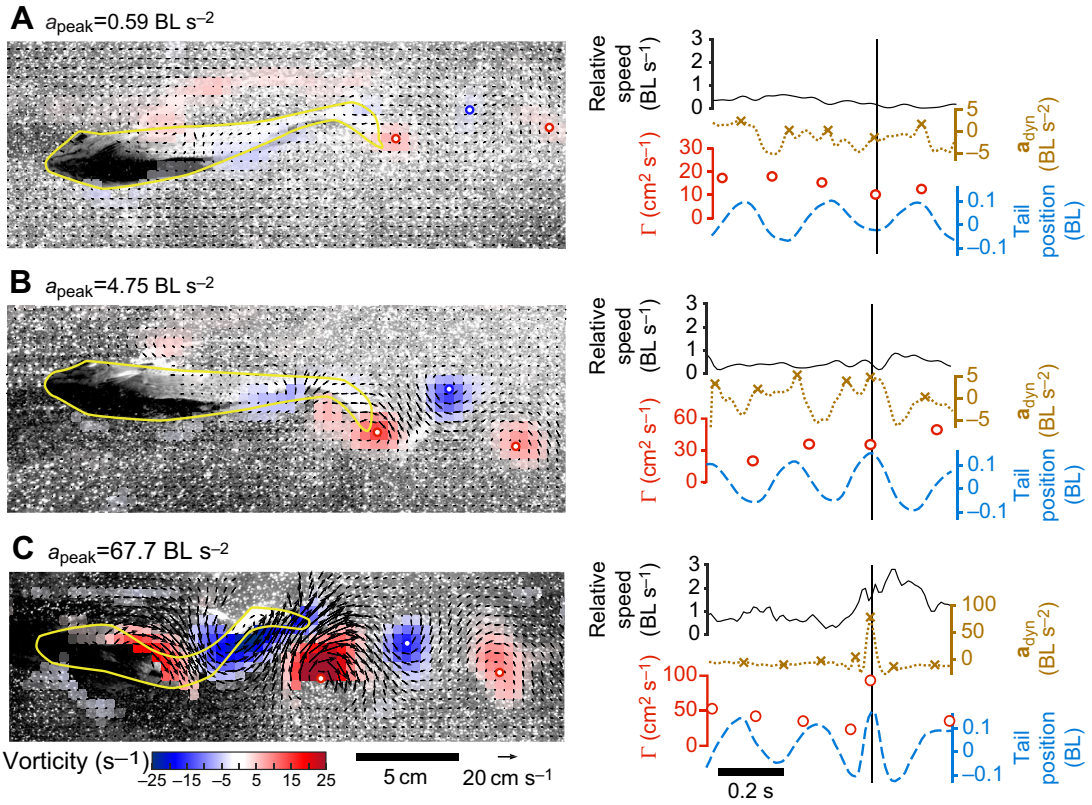

Fig. 3. Example flow fields, kinematic data and acceleration measurements. Ventral video frames, vorticity (in color) and velocity vectors (black arrows) for the same individual swimming steadily (A), and accelerating at a medium (B) and high rate (C), starting at an initial swimming speed of 1.5 BL s^{-1} in each case. Color indicates vorticity, with red and blue circles to indicate the centers of each vortex. The panels on the right show the speed relative to the laboratory (black), the dynamic acceleration $\mathbf{a}_{dyn}$ (brown, dotted) with brown crosses marking the peak acceleration a_{peak} for each half tail beat, the magnitude of the most recently shed vortex's circulation (red circles), and the position of the tail (blue, dashed). The vertical line indicates the time of the frame shown on the left.

Journal of Experimental Biology (2018) 221, jeb190892. doi:10.1242/jeb.190892

indicated by the velocity vectors, shown in black. Vorticity is higher and jets are stronger in the high acceleration sequence (Fig. 3C). The right panels of Fig. 3 show raw kinematic and acceleration data. Note that the acceleration (brown) has two peaks per tail beat cycle, which are marked with crosses and are seen most clearly in Fig. 3A,B. This is expected because tail movements to the left side should produce a symmetrical forward acceleration as tail movements to the right. Higher accelerations correspond to increases in vortex circulation (red circles) and to changes in tail beat frequency. Amplitude also increases during acceleration, but less than frequency (see, particularly, the amplitude and frequency near the peak in acceleration in Fig. 3C). Additionally, the unsteady sequences (Fig. 3B,C; Movies 2 and 3) have higher tail beat amplitude overall than the steady sequence (Fig. 3A; Movie 1), even though most of the acceleration peaks in Fig. 3B (brown crosses) are of similar magnitude to those in Fig. 3A.

Wake structure and force production

We compared the total force produced during steady and unsteady sequences with different magnitudes of acceleration, starting from different steady swimming speeds (Fig. 4). On average, force increases significantly in higher acceleration bins (P<0.0001; Table S1), and is significantly higher in unsteady sequences compared with steady ones (P<0.0001). Force also increases across swimming speeds (P<0.0001), with the force at each flow speed significantly different from the force at all other speeds. The forces for unsteady high acceleration tail beats are at least 2.24 times the forces for steady zero acceleration tail beats (at 1.5 BL s^{-1}) and are as much as 7.40 times (at 1.0 BL s^{-1}) (Fig. 4).

Based on these results, we can estimate the added mass and drag coefficients using Eqns 2–4. The drag coefficient can be estimated from the steady tail beats in the zero acceleration bin. In this case, we assume that the force to accelerate is zero, so that $C_D \approx \mathbf{F}_{axial}/\left(\frac{1}{2}\rho S U^2\right)$. Fig. 5A shows the drag coefficient relative to speed. The overall median drag coefficient is 0.0042. For the added mass coefficient, we first estimate the drag force from Eqn 4, using the median drag coefficient at each swimming speed. Then, we use Eqns 2 and 3 to estimate C_A. We find that the median added mass coefficient is always higher in unsteady tail beats, and that it tends to decrease as the acceleration increases (Fig. 5B). It also tends to be higher for accelerations from higher swimming speeds, so that the largest coefficient (0.78) is for low accelerations from 2.0 BL s^{-1} and the smallest (0.04) is for high accelerations from 1.5 BL s^{-1}.

The angle of vortex pairs in the wake increases slightly as acceleration increases (Fig. 6). The angle is significantly different among acceleration categories (P=0.0084; Table S1), but does not change significantly between steady and unsteady sequences (P=0.0522). Although there is a significant effect of acceleration, the magnitude of the effect is small; the largest difference is between zero and high acceleration, but it is only 4.8±1.3 deg.

The vortex ring diameter is significantly smaller for unsteady sequences compared with steady ones (P=0.0006; Table S1). Fig. 7 shows the horizontal vortex ring diameter D normalized relative to its vertical diameter d, which we assume is equal to the height of the fish's tail. This diameter also decreases significantly as flow speed increases (P<0.0001). A value of d/D equal to one indicates a circular ring, and in all cases, the measured value is not significantly different from 1 (P>0.099), except for the zero acceleration case at 1 BL s^{-1}, in which d/D=1.24±0.06, which is significantly larger than 1 (P=0.0293).

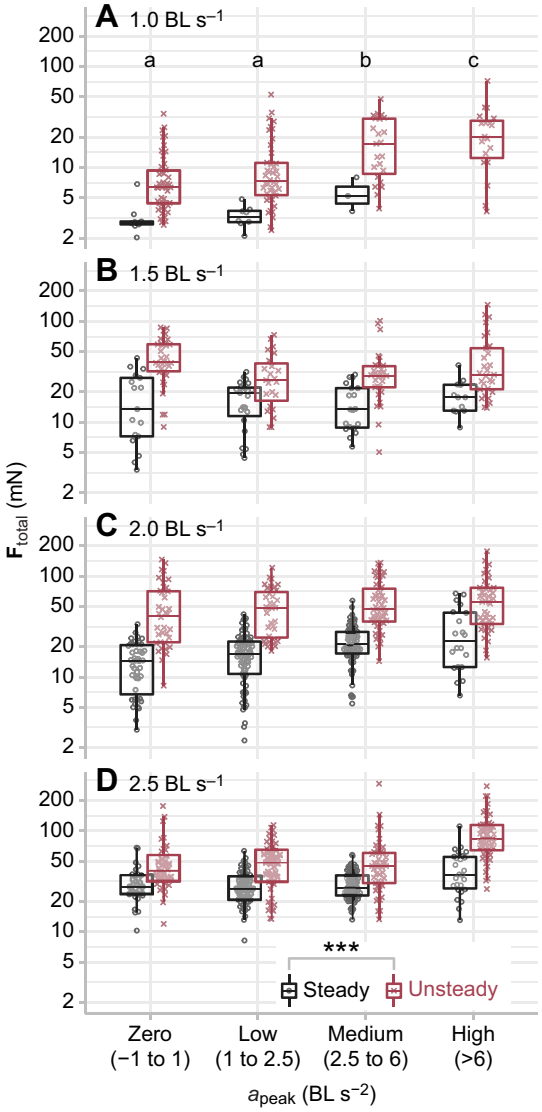

Fig. 4. Total force increases in unsteady sequences and with increasing acceleration and swimming speed. Total force in the four different acceleration categories at swimming speeds of (A) 1.0 BL s^{-1}, (B) 1.5 BL s^{-1}, (C) 2.0 BL s^{-1} and (D) 2.5 BL s^{-1}. Points are jittered to avoid overlap. Acceleration categories that are labeled with different letters have forces that are significantly different from one another (P<0.05), averaged across all swimming speeds. ***P<0.0001, averaged across other categories.

Kinematic changes during acceleration

Tail beat frequency increases with both flow speed and acceleration, and is higher in unsteady tail beats compared with steady ones (Fig. 8). Tail beat frequency changes significantly across acceleration categories (P<0.0001; Table S2) and across flow speeds (P<0.0001). It is also significantly higher in unsteady tail beats than in steady ones (P<0.0001); unsteady tail beats have a tail beat frequency 1.05±0.51 Hz higher than steady ones, on average. There is also a significant interaction between acceleration and flow speed (P=0.0002), so that the highest tail beat frequencies occur at 2.5 BL s^{-1} and high acceleration.

Head and tail amplitude are significantly higher during unsteady tail beats than during steady ones (Fig. 9; $P \leq 0.0003$; Table S2). On average, head and tail amplitudes are 0.0037±0.0007 BL and 0.015±0.001 BL higher, respectively, in unsteady tail beats than steady. Amplitudes are also significantly different among

Journal of Experimental Biology (2018) 221, jeb190892. doi:10.1242/jeb.190892

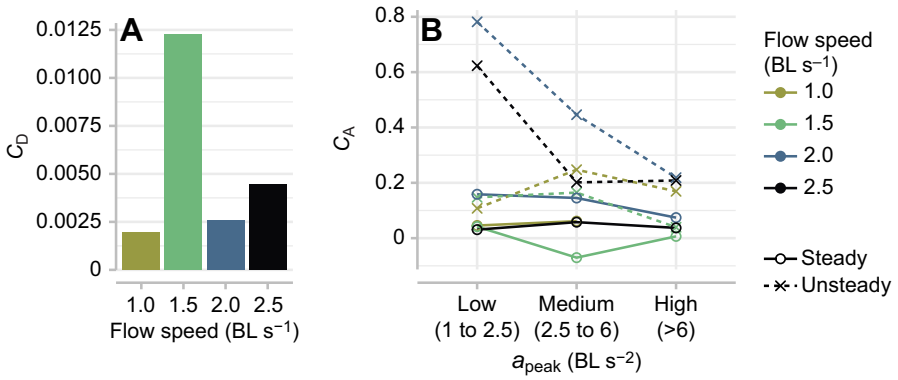

Fig. 5. The median added mass coefficient is higher in unsteady sequences and decreases as acceleration increases. (A) The median drag coefficient C_D plotted against flow speed. (B) The median added mass coefficient C_A plotted against acceleration groups, where color indicates the flow speed.

acceleration categories (P<0.0001 in both cases), but only the high acceleration category has significantly larger amplitudes than the others. They both also increase significantly as flow speed increases (P<0.0001 in both cases). Tail amplitude is significantly different at each flow speed, while head amplitude at the 1 and 1.5 BL s^{-1} is significantly different from head amplitude at 2.0 and 2.5 BL s^{-1}.

The total force is strongly correlated with the frequency and amplitude. The correlation coefficient between log force and frequency is 0.74, between log force and tail amplitude is 0.38, and between log force and head amplitude is 0.19. Most of these correlations are related to the changes in vortex circulation, not the changes in vortex diameter. Vortex diameter is best associated with tail amplitude, but the correlation coefficient is only 0.14.

DISCUSSION

During steady swimming, fish produce a wake that contains regularly spaced vortex pairs (Lauder and Tytell, 2005). The circulation and orientation of these vortices reflect the forces the fish produces for swimming, which include both lateral and axial components. To accelerate, fish must produce more axial force than it would during steady swimming. The axial force could be increased by redirecting the same total force so that it points more posteriorly (Fig. 1B), by increasing the total force output so that the axial component is greater (Fig. 1C), or both. If the angle of the vortex pairs in the wake changes, that would indicate a change in the direction of the force, and if the circulation of the vortices changes, that would indicate a change in the magnitude of the force. Eels change the direction of the force when they accelerate, indicated by a change in the orientation of vortices in their wakes to accelerate (Tytell, 2004a). Trout change both the orientation and strength of vortices in their wake (Akanyeti et al., 2017). Because the bluegill has a stiffer body than the eel or the trout (Aleyev, 1977), we predicted that it would be less able to curve its body in order to redirect forces and manipulate the locations of vortices in its wake. Instead, we predicted that it would increase the circulation of vortices in the wake, increasing the total force. Our data partially support our hypothesis. The bluegill substantially increased circulation of vortices in the wake (Fig. 4), leading to an increase in total force as acceleration strength increased. It also significantly increased the angle of the vortex pairs, but to a much smaller degree (Fig. 6).

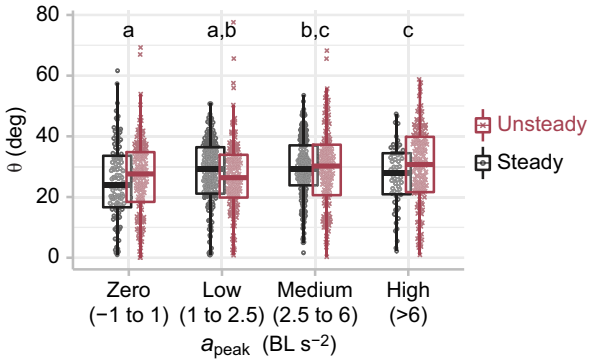

Fig. 6. The angle of the vortex ring in the wake increases with increasing acceleration, but is not different among steady and unsteady sequences. The angle of the first vortex pair relative to the swimming direction is plotted against acceleration categories for steady (black) and unsteady (red) sequences. Points are jittered to avoid overlap. Acceleration categories labeled with different letters have angles that are significantly different from one another (P<0.05).

Even though bluegill change both the magnitude and direction of force during acceleration, the most important effect is the change in magnitude. The angle of the vortex ring in the wake and the total force it represents allows an estimate of the axial force (Eqn 1). Axial force increases from 4.2 mN in the steady, zero acceleration case to 21.9 mN in the unsteady, high acceleration case. If the vortex ring angle did not change over this range, the change in total force would still account for 78% of the total increase in axial force. If the vortex ring angle changed, but the total force stayed constant, then the axial force would only increase to 24% of its unsteady, high acceleration value. Thus, as we hypothesized, the primary way the bluegill accelerates is to increase the force it produces, not by redirecting the force or changing the structure of its wake.

This pattern is different from the changes in the wakes of accelerating eels (Tytell, 2004a). Steadily swimming eels produce lateral jets in their wake, with very little downstream momentum, as is required by the zero net force on the body during steady swimming (Tytell and Lauder, 2004). As eels accelerate, they change the structure of their wake, rotating the jets to point backwards, which provides the extra force needed to accelerate (Tytell, 2004a). The eels do not substantially change the circulation of the vortices in the wake.

Koi carp (*Cyprinus carpio*) may accelerate using a combination of these two patterns. Wu et al. (2007) studied burst-and-coast swimming and compared bursts with a single tail flick to one side to those with multiple tail flicks. When bursting with a single tail flick, they change the angle of the vortex pair substantially compared to a burst with multiple tail flicks (Wu et al., 2007). They do not report any data from steady swimming, so it is not possible to ascertain if the vortex circulation was higher during acceleration compared to steady swimming.

Journal of Experimental Biology (2018) 221, jeb190892. doi:10.1242/jeb.190892

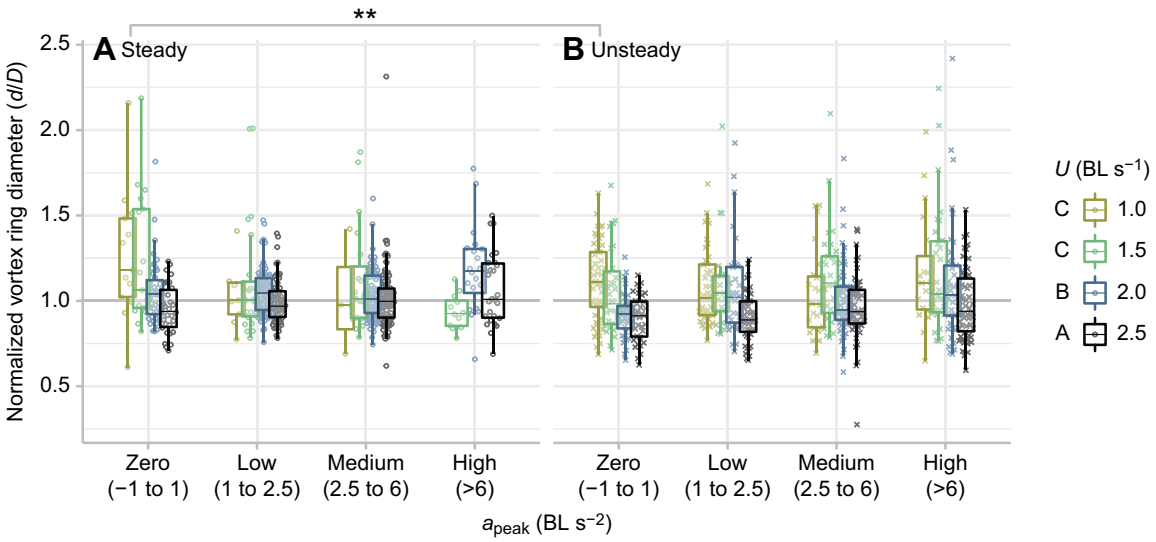

Fig. 7. The ratio of the horizontal vortex ring diameter (*D*) to the vertical diameter (*d*) is significantly smaller in unsteady sequences and at higher swimming speeds, but does not change significantly with acceleration. Normalized vortex ring diameter is plotted against acceleration categories for steady (A) and unsteady (B) sequences. The vortex ring diameter in the horizontal plane *D* is normalized by the tail height *d*. A value of 1 indicates a circular ring. Points are jittered to avoid overlap. In the key, speeds labeled with different letters have vortex ring diameters that are significantly different ($P<0.05$). **$P<0.001$.

The kinematic changes we observed are consistent with those described by Akanyeti et al. (2017), who performed a large survey of acceleration in many species of fishes. They found that tail beat amplitude increased by 34%, on average, across all species during acceleration, relative to steady swimming. In our data, the tail beat amplitude during the unsteady, high acceleration case is 33±15% higher than the steady, zero acceleration case (Fig. 9). Akanyeti et al. also reported that tail beat frequency increased with acceleration and with swimming speed, but that acceleration was the stronger effect, the same pattern that we observed (Fig. 8).

However, our wake flow data are different from those of Akanyeti et al. (2017). They hypothesized that accelerating fishes modulate the vortex ring size and orientation to increase propulsive efficiency, but our data do not support this hypothesis. They performed detailed wake analysis from rainbow trout (*Oncorhynchus mykiss*) during acceleration and found that vortex ring impulse increased dramatically, the vortex ring jet reoriented substantially more downstream, and the rings became more circular. In our data, we found a similar increase in impulse. For trout, the impulse increased 3.25 times (based on fig. 4C in Akanyeti et al., 2017). We found that the median impulse in the unsteady, high acceleration case was 2.1 times the value in the steady, zero acceleration case. We did not find a substantial change in vortex angle (only 4.8±1.3 deg), while Akanyeti et al. reported a change of 28 deg (based on fig. 4C in Akanyeti et al., 2017). We found no support for the idea that vortex rings become more circular during acceleration. Bluegill vortex rings are not significantly different from circular at nearly all combinations of flow speed and acceleration. Trout produce oval-

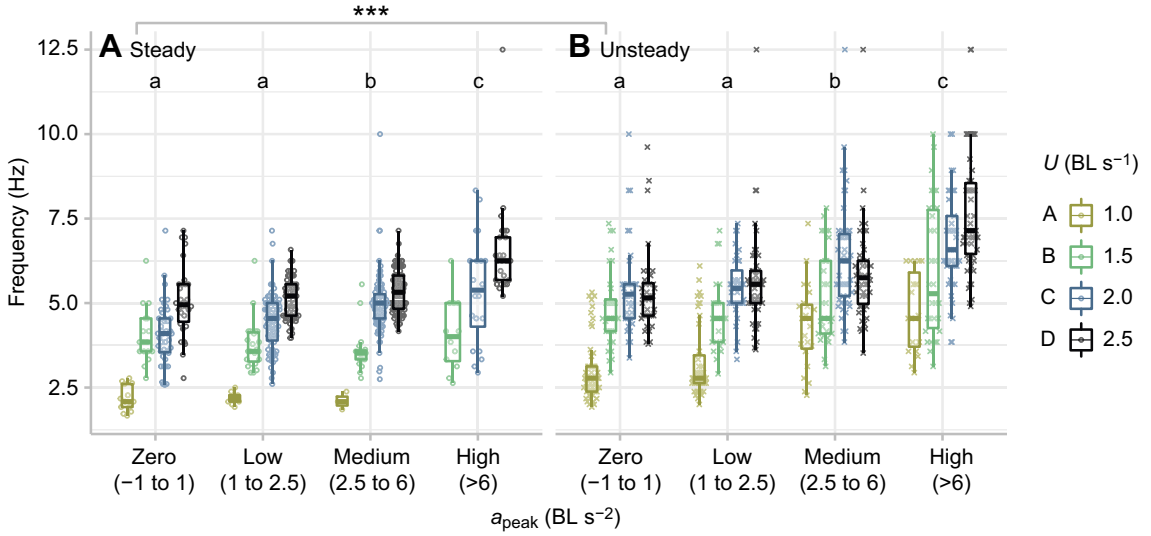

Fig. 8. Tail beat frequency is higher in unsteady sequences and increases with both acceleration and swimming speed. Tail beat frequency is plotted against acceleration categories for steady (A) and unsteady (B) sequences. Points are jittered to avoid overlap. Groups that have significantly different frequencies ($P<0.05$) are labeled with different letters, with lowercase letters indicating significant differences across acceleration categories and uppercase letters indicating significant differences across swimming speeds. ***$P<0.0001$.

Journal of Experimental Biology (2018) 221, jeb190892. doi:10.1242/jeb.190892

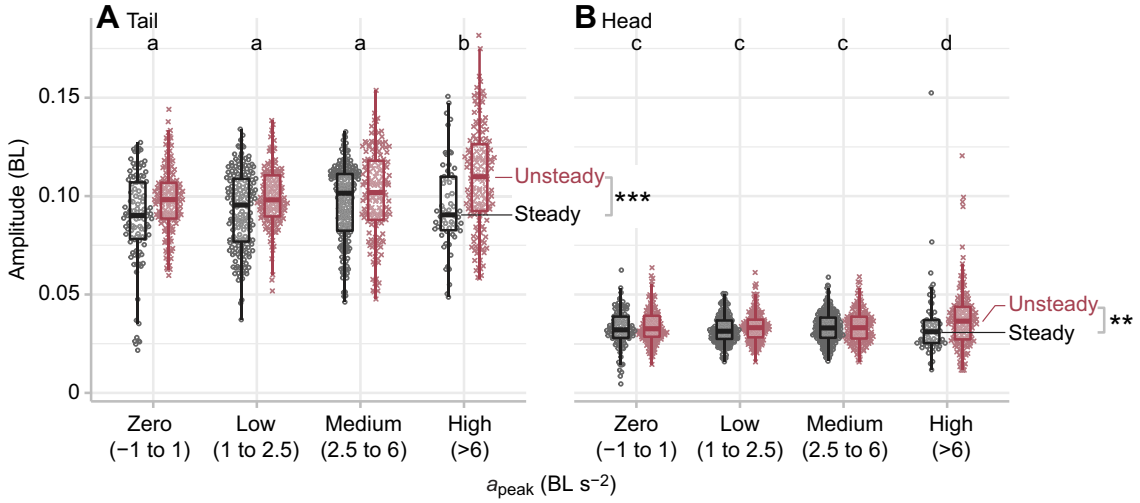

Fig. 9. Both head and tail amplitude increase in unsteady sequences and at the highest accelerations. Tail amplitude (A) and head amplitude (B) are plotted against acceleration categories for steady sequences (black) and unsteady sequences (red). Points are jittered to avoid overlap. Acceleration categories labeled with different letters have amplitudes that are significantly different from one another (P<0.05). **P<0.001; ***P<0.0001.

shaped rings during steady swimming (d/D<1 and decrease the horizontal diameter D during acceleration, so that d/D becomes closer to 1. Bluegill show the opposite pattern: d/D starts out higher during steady tail beats and decreases during unsteady ones.

Steady and unsteady tail beats

Even in trials in which the fish swam steadily, we found a range of acceleration magnitudes (Fig. 2). As part of the experimental procedure, we performed trials in which we elicited accelerations, and performed other trials in which we worked with the fish until it swam steadily for at least five full tail beats. Steady swimming was straightforward to assess because the fish were swimming against a steady flow in a flow tank. When the fish matched the flow speed, the image in the video would remain in the same place over several tail beats, moving less than 2% of its body length within the flow tank. For steady and unsteady tail beats, we measured the acceleration using the IMU. Every tail beat produces a small acceleration and a small deceleration, even when the fish is swimming steadily on average (Borazjani, 2015; Plew et al., 2007; Tytell, 2007; Wen and Lauder, 2013; Xiong and Lauder, 2014), and the range of accelerations increases at higher steady swimming speeds (Plew et al., 2007; Xiong and Lauder, 2014). Most of the steady tail beats had zero or low acceleration (Fig. 2), but there was still a range of acceleration magnitudes, and the range of accelerations increased as the swimming speed increased, similar to what Xiong and Lauder (2014) reported. In unsteady tail beats, however, the distribution of acceleration values that we measured did not vary substantially across swimming speeds.

The primary difference between steady and unsteady tail beats is that, in unsteady tail beats, the fish maintains an acceleration over several tail beats. A steady trial may have a tail beat with a strong forward acceleration, but it is followed by a tail beat with a similar deceleration, so that the overall speed does not change. In unsteady tail beats, a strong acceleration in one tail beat is sustained over several more, so that the overall speed increases.

Because of this range of accelerations, we could compare steady and unsteady tail beats with the same acceleration magnitude. Surprisingly, the fish produced substantially higher forces during unsteady tail beats than during steady ones, even at the same acceleration (Fig. 4). How could this be possible? We suggest that the extra force is needed to overcome fluid dynamic added mass (Faber, 1995), and that the added mass coefficient increases when both tail beat amplitude and frequency increase. When a fish is actively trying to accelerate, it must overcome the fluid dynamic acceleration reaction, also called added mass (Daniel, 1984; Faber, 1995). To accelerate in a fluid, a fish must accelerate its own mass and some fluid around it, an effect called the acceleration reaction. The added mass coefficient C_A describes the strength of this effect, and is typically 1.0 or less for streamlined bodies (Daniel, 1984). Based on our data, we estimated added mass coefficients for the bluegill (Fig. 5B). These coefficients were always higher for unsteady tail beats, in which acceleration was sustained over several tail beats, compared with steady tail beats, and they decreased with increasing acceleration.

We suggest that the reason for the increase in force in unsteady tail beats is that higher tail beat amplitudes and frequencies increase the added mass coefficient. If the body amplitude is higher, then the amount of fluid that must be accelerated with the body is also higher. At higher tail beat frequencies, the side-to-side acceleration of the body is also higher, by definition (see also Bale et al., 2014b). Each time the tail beats, the fish accelerates forward (Tytell, 2007; Xiong and Lauder, 2014). At a higher tail beat frequency, these small accelerations occur more frequently, potentially leading to a greater impact from the acceleration reaction over the course of multiple tail beats.

Note that this acceleration reaction is somewhat different from the one traditionally discussed in fluid dynamics textbooks (e.g. Smits, 2000). The acceleration reaction is often discussed as the increase in force in a particular direction due to acceleration in the same direction. In a full description, however, the added mass coefficient is a 3×3 tensor, where the diagonal elements indicate the extra force in one direction required to accelerate in the same direction. The added mass coefficient we have estimated, however, includes components both from the traditional acceleration reaction and from an off-diagonal element: an increase in forward force required due to the side-to-side acceleration of the tail.

We found that head and tail amplitude both increased by ∼12–32% in unsteady tail beats, relative to steady tail beats (Fig. 8), at the same swimming speed. Frequency increased by 1.05±0.51 Hz in unsteady tail beats. Both of these increases could increase the added

Journal of Experimental Biology (2018) 221, jeb190892. doi:10.1242/jeb.190892

mass. Tytell (2004a) estimated the added mass coefficient for accelerating eels and found that it was as high as 2.8 during accelerations. Similarly, Wu et al. (2007) estimated the drag coefficient on carp during acceleration and found that it was about four times higher than the drag during gliding. However, they assumed a constant added mass coefficient. Their results could also be explained by an increase in added mass during acceleration, as they acknowledge (Wu et al., 2007).

It is also possible to interpret this additional force requirement during acceleration in unsteady tail beats as an increase in the drag coefficient. From our data, it is not possible to separate an increase in drag coefficient during acceleration and an increase in the added mass coefficient. Because the effect is associated with acceleration, we have chosen to interpret it as an added mass coefficient. Regardless of the interpretation, it is clear from our data that bluegill require more axial force to sustain an acceleration over several tail beats than they require to produce the same acceleration during an otherwise steady swimming sequence. This is particularly evident in the forces at 1.5 BL s^{-1}. The estimated drag coefficient at 1.5 BL s^{-1} was higher than at other speeds. The axial force for some tail beats was particularly high at 1.5 BL s^{-1}, because the wake forces were high and the vortex ring angles were higher, which led to a higher estimated drag coefficient. This may be due to differences in swimming patterns for different individuals. At 1.5 BL s^{-1}, most individuals were using both their pectoral fins and tail for swimming. It is possible that the measured force was higher because of interactions between the pectoral fin wake and the tail wake, which may have caused the angle of the wake vortex rings to shift. Because of this high drag coefficient, the estimated added mass coefficient for steady swimming at 1.5 BL s^{-1} is low, and even becomes negative for medium accelerations. Combining the drag and acceleration forces, however, means that the force required to accelerate at 1.5 BL s^{-1} shows a similar pattern as the forces at other speeds (Fig. 4).

Kinematics during accelerations

Relatively few studies have quantified how kinematics change as a function of the magnitude of an acceleration. Like the current results, Tytell (2004a) found that eels accelerate by increasing both head and tail amplitude proportionally to acceleration. Bluegill also increase amplitude during accelerations, compared with steady swimming, but the increase is not proportional to the acceleration (Fig. 9). Eels also increase tail beat frequency during acceleration (Tytell, 2004a), much like bluegill in our study (Fig. 8).

Acceleration performance is related to increases in amplitude across the whole body (Akanyeti et al., 2017). Across a wide range of species, Akanyeti et al. (2017) found that undulatory amplitudes increased during acceleration by about 34% on average across 51 species, which is very close to the 33% that we found in unsteady, high accelerations. Similarly, Wen et al. (2012) and Borazjani and Sotiropoulos (2010) studied the swimming performance of robotic and computational models as they accelerated from rest to a steady state, comparing the performance of anguilliform (eel-like) and carangiform (mackerel-like) kinematics. For the same tail amplitude, anguilliform swimmers have higher anterior body amplitude, and both studies found that these kinematics cause more rapid initial acceleration, even though their final swimming speed is lower (Borazjani and Sotiropoulos, 2010; Wen et al., 2012). These models thus suggest that carangiform swimmers, like bluegill, can accelerate faster by adopting a more eel-like swimming mode with greater head amplitude, which is what our data show (Fig. 9).

We also found that frequency increases proportionally to both swimming speed and acceleration (Fig. 8), but that the increase for acceleration is larger than the increase for swimming speed. This is similar to the pattern that Akanyeti et al. (2017) reported for rainbow trout.

Contributions of other fins to acceleration

In this study, we examined the contribution of only the caudal fin to thrust, but, clearly, other fins also contribute to thrust. Although we did not quantify it, one can observe from our videos that bluegill tend to beat their pectoral fins at the beginning of an acceleration. Thus, the force we measured off the caudal fin is not the total force on the entire body. The role of the pectoral fin should diminish as flow speed increases. However, as the steady swimming speed increases, pectoral fin forces are directed more laterally, so their contribution to thrust might decrease (Drucker and Lauder, 2000). The angle between the force vector and the swimming direction increases to around 86 deg as flow speeds increase past 1.5 BL s^{-1} (Drucker and Lauder, 2000). It is not known whether the pectoral fins re-orient their forces to produce more thrust during acceleration. If the pattern seen during steady locomotion remains during accelerations, then the pectoral fins should produce very little axial force in comparison to the caudal fin.

The dorsal and anal fin may also produce significant thrust forces during accelerations. These fins have been shown to produce significant amounts of force once flow speed surpasses 1.1 BL s^{-1}. The dorsal fin alone can produce 12% of total thrust during steady swimming (Drucker and Lauder, 2001). The anal fin may have similar thrust patterns (Tytell, 2006). It seems likely that these median fins are also important for thrust during acceleration. Wen et al. (2018) recently considered acceleration in a soft robotic device. They found that erecting median fins in their robot increased the initial axial force and, somewhat counter-intuitively, decreased the side forces (Wen et al., 2018). It seems likely that the bluegill in this study may have been using their median fins in a similar way to those in Wen's study.

Individual fish may partition forces among their fins differently. We observed that certain fish used their pectoral and caudal fins at different times. Some of the fish used their pectoral fins very infrequently, and others did not. If these other fins produce different amounts of force in different individuals, it could explain the large variation of force produced by the caudal fin for a given acceleration (Fig. 4). We found that individuals varied significantly in how much force they produced and how the force changed from steady to unsteady tail beats, even though the individuals were all of similar size. This variation could be a result of individuals relying on different fins for the same thrust requirements.

Efficiency and stability during acceleration

We found that bluegill accelerate primarily by increasing the total force in their wake (Fig. 4) and only secondarily by changing the angle of vortex pairs (Fig. 6). However, altering the angle would be a more energetically efficient way to accelerate. If bluegill could simply reorient the vortex rings in the wake so that more of the force was directed backwards, then they would not have to expend more energy to create stronger vortices with higher circulation. To change the vortex ring orientation, the bluegill would have to change the lateral spacing of vortices relative to the distance it travels forward in a single tail beat (called the 'stride length') (Videler, 1993). In Fig. 1B, the lateral spacing is the same as Fig. 1A, but the axial distance between vortices is less. Alternatively, bluegill could increase the lateral spacing of vortices while keeping the stride length constant.

However, physics may constrain how much the bluegill can change the geometry of its wake. It may not be able to change its stride length independently of the spacing of vortices in its wake. If it were able to increase the angle of vortices in its wake by decreasing the stride length, then more of the vortex momentum would be aligned in the axial direction, which would tend to increase the stride length. Similarly, if it increased the lateral spacing of vortices while keeping stride length constant, then the central jet between them would be larger and would contain more momentum, which would tend to increase the stride length. Additionally, the bluegill's body may not be flexible enough to manipulate its wake structure, like the eel does (Tytell, 2004a). In particular, it would have to flex its tail more to increase the lateral spacing of vortices. Thus, the bluegill's body mechanics and the physics of propulsion may limit how much it can alter its wake for acceleration.

Even if the bluegill was capable of reorienting vortices in its wake, doing so might sacrifice stability. Reorientation would result in more axial force from the caudal fin, but would also result in smaller lateral forces. At higher flow speeds, bluegills increase lateral forces from the pectoral fins to increase stability during steady swimming (Fish and Lauder, 2006). Similarly, lateral forces from the caudal fin could also help to stabilize the fish. Lateral stabilizing forces may be particularly important during acceleration, because the movement is inherently unstable. The caudal fin produces a large forward force, but it is located behind the center of mass. Much like backing up a car with a trailer attached, this situation represents an unstable equilibrium. Active lateral stabilization may therefore be particularly important during acceleration.

Conclusions

Bluegill sunfish accelerate by increasing the total amount of force produced during each tail beat, but do not substantially redirect the force produced. This process increases the total amount of axial force, allowing for acceleration, but does not lead to a dramatic reconfiguration of the wake structure, as seen for acceleration by eels (Tytell, 2004a). The bluegill may be constrained by its relatively stiff body, as well as the physics of propulsion in a fluid, to produce the same sort of wake during steady swimming and acceleration. Similarly, the consistent lateral and axial forces shed by the tail may be necessary in order to stabilize the moving fish. Surprisingly, for the same magnitude acceleration, we found that bluegill produce much lower forces during a single steady tail beat than within an acceleration sequence that lasts for several tail beats. We attribute this difference to the increase in amplitude during sustained accelerations, which is required to produce higher forces, but also increases the added mass coefficient on the fish.

Acknowledgements

The authors thank Alexandra Boden for help in running the experiments and Vishesh Vikas with help setting up the IMUs.

Competing interests

The authors declare no competing or financial interests.

Author contributions

Conceptualization: E.D.T., T.N.W., M.A.B.S.; Methodology: T.N.W., E.D.T., M.A.B.S.; Software: E.D.T.; Formal analysis: E.D.T.; Investigation: T.N.W., M.A.B.S.; Data curation: E.D.T.; Writing - original draft: T.N.W.; Writing - review & editing: M.A.B.S., E.D.T.; Visualization: T.N.W.; Supervision: M.A.B.S., E.D.T.; Project administration: E.D.T.; Funding acquisition: E.D.T.

Funding

This material is based upon work supported by, or in part by, the US Army Research Laboratory and the US Army Research Office under contract/grant number W911NF-14-1-0494 and W911NF-14-1-0268. Additional support was received from the National Science Foundation under grant DBI-RCN 1062052 (to L. J. Fauci and A. H. Cohen) and the National Institute of Health Training in Education and Critical Research Skills under grant number K12GM074869 (to M.A.B.S). Deposited in PMC for release after 12 months.

Data availability

Raw video data are available from ZMAPortal (https://zmaportal.org) study ZMA18. Notes, code, processed data and analysis notebooks are available at doi:10.6070/H4KS6Q5V.

Supplementary information

Supplementary information available online at http://jeb.biologists.org/lookup/doi/10.1242/jeb.190892.supplemental

References

Akanyeti, O., Putney, J., Yanagitsuru, Y. R., Lauder, G. V., Stewart, W. J., Liao, J. C. and Russell, D. W. (2017). Accelerating fishes increase propulsive efficiency by modulating vortex ring geometry. *Proc. Natl. Acad. Sci USA* **114**, 13828-13833.

Aleyev, Y. G. (1977). *Nekton*. The Hague: Junk.

Bale, R., Shirgaonkar, A. A., Neveln, I. D., Bhalla, A. P. S., MacIver, M. A. and Patankar, N. A. (2014a). Separability of drag and thrust in undulatory animals and machines. *Sci. Rep.* **4**, 7329.

Bale, R., Hao, M., Bhalla, A. P. S., Bhalla, S. and Patankar, N. A. (2014b). Energy efficiency and allometry of movement of swimming and flying animals. *Proc. Natl. Acad. Sci. USA* **111**, 7517-7521.

Borazjani, I. (2015). Simulations of unsteady aquatic locomotion: from unsteadiness in straight-line swimming to fast-starts. *Integr. Comp. Biol.* **55**, 740-752.

Borazjani, I. and Sotiropoulos, F. (2008). Numerical investigation of the hydrodynamics of carangiform swimming in the transitional and inertial flow regimes. *J. Exp. Biol.* **211**, 1541-1558.

Borazjani, I. and Sotiropoulos, F. (2010). On the role of form and kinematics on the hydrodynamics of self-propelled body/caudal fin swimming. *J. Exp. Biol.* **213**, 89-107.

Daniel, T. L. (1984). Unsteady aspects of aquatic locomotion. *Integr. Comp. Biol.* **24**, 121-134.

Domenici, P. and Blake, R. W. (1997). The kinematics and performance of fish fast-start swimming. *J. Exp. Biol.* **200**, 1165-1178.

Drucker, E. G. and Lauder, G. V. (2000). A hydrodynamic analysis of fish swimming speed: wake structure and locomotor force in slow and fast labriform swimmers. *J. Exp. Biol.* **203**, 2379-2393.

Drucker, E. G. and Lauder, G. V. (2001). Locomotor function of the dorsal fin in teleost fishes: experimental analysis of wake forces in sunfish. *J. Exp. Biol.* **204**, 2943-2958.

DuBois, A. B. (1978). Forces on the tail surface of swimming fish: thrust, drag and acceleration in bluefish (*Pomatomus saltatrix*). *J. Exp. Biol.* **77**, 225-241.

DuBois, A. B., Cavagna, G. A. and Fox, R. S. (1974). Pressure distribution on the body surface of swimming fish. *J. Exp. Biol.* **60**, 581-591.

Faber, T. E. (1995). *Fluid dynamics for physicists*. Cambridge: Cambridge University Press.

Fernández-Prats, R., Raspa, V., Thiria, B., Huera-Huarte, F. and Godoy-Diana, R. (2015). Large-amplitude undulatory swimming near a wall. *Bioinspir. Biomim.* **10**, 016003.

Fish, F. E. and Lauder, G. V. (2006). Passive and active flow control by swimming fishes and mammals. *Annu. Rev. Fluid Mech.* **38**, 193-224.

Kloke, J. and McKean, J. W. (2015). *Nonparametric Statistical Methods Using R*. Boca Raton: CRC Press.

Koochesfahani, M. M. (1989). Vortical patterns in the wake of an oscillating airfoil. *AIAA J.* **27**, 1200-1205.

Lauder, G. V. and Tytell, E. D. (2005). Hydrodynamics of Undulatory Propulsion. In *Fish Physiology* (ed. R. E. Shadwick and G. V. Lauder), pp. 425-468. San Diego: Elsevier Academic Press.

Lauder, G. V., Drucker, E. G. and Nauen, J. C. (2003). Experimental hydrodynamics and evolution: caudal fin locomotion in fishes. In *Vertebrate Biomechanics and Evolution* (ed. V. L. Bels, J.-P. Gasc and A. Casinos), pp. 117-135. Oxford: BIOS Scientific Publishers.

Lighthill, M. J. (1970). Aquatic animal propulsion of high hydromechanical efficiency. *J. Fluid Mech.* **44**, 265-301.

Madgwick, S. O. H., Harrison, A. J. L. and Vaidyanathan, A. (2011). Estimation of IMU and MARG orientation using a gradient descent algorithm. *IEEE Int. Conf. Rehabil. Robot.* **2011**, 5975346-5975347.

Plew, D. R., Nikora, V. I., Larned, S. T., Sykes, J. R. E. and Cooper, G. G. (2007). Fish swimming speed variability at constant flow: *Galaxias maculatus*. *New Zeal. J. Mar. Freshw. Res.* **41**, 185-195.

Smits, A. J. (2000). *A Physical Introduction to Fluid Mechanics*. New York: John Wiley and Sons.

Tytell, E. D. (2004a). Kinematics and hydrodynamics of linear acceleration in eels, *Anguilla rostrata*. *Proc. R. Soc. London B* **271**, 2535-2541.

Tytell, E. D. (2004b). The hydrodynamics of eel swimming. II. Effect of swimming speed. *J. Exp. Biol.* **207**, 3265-3279.
Tytell, E. D. (2006). Median fin function in bluegill sunfish, *Lepomis macrochirus*: streamwise vortex structure during steady swimming. *J. Exp. Biol.* **209**, 1516-1534.
Tytell, E. D. (2007). Do trout swim better than eels? Challenges for estimating performance based on the wake of self-propelled bodies. *Exp. Fluids* **43**, 701-712.
Tytell, E. D. (2011). Experimental hydrodynamics. In *Encyclopedia of Fish Physiology: From Genome to Environment* (ed. A. P. Farrell), pp. 535-546. San Diego: Elsevier.
Tytell, E. D. and Lauder, G. V. (2004). The hydrodynamics of eel swimming. I. Wake structure. *J. Exp. Biol.* **207**, 1825-1841.
Videler, J. J. (1993). *Fish Swimming*. London: Chapman and Hall.
Webb, P. W. (1991). Composition and mechanics of routine swimming of rainbow trout, *Oncorhynchus mykiss*. *Can. J. Fish. Aquat. Sci.* **48**, 583-590.
Wen, L. and Lauder, G. V. (2013). Understanding undulatory locomotion in fishes using an inertia-compensated flapping foil robotic device. *Bioinspir. Biomim.* **8**, 46013.
Wen, L., Wang, T. M., Wu, G. and Liang, J. H. (2012). Hydrodynamic investigation of a self-propelled robotic fish based on a force-feedback control method. *Bioinspir. Biomim.* **7**, 36012.
Wen, L., Ren, Z., Di Santo, V., Hu, K., Yuan, T., Wang, T. and Lauder, G. V. (2018). Understanding fish linear acceleration using an undulatory biorobotic model with soft fluidic elastomer actuated morphing median fins. *Soft Robot* **5**, 375-388.
Wickham, H. (2009). *ggplot2: Elegant Graphics for Data Analysis*. New York: Springer-Verlag.
Wu, G., Yang, Y. and Zeng, L. (2007). Kinematics, hydrodynamics and energetic advantages of burst-and-coast swimming of koi carps (*Cyprinus carpio* koi). *J. Exp. Biol.* **210**, 2181-2191.
Xiong, G. and Lauder, G. V. (2014). Center of mass motion in swimming fish: effects of speed and locomotor mode during undulatory propulsion. *Zoology* **117**, 269-281.